AGU PUBLICATIONS

JGR

Journal of Geophysical Research: Space Physics

RESEARCH ARTICLE
10.1002/2016JA023792

Key Points:
- Saturn's dawn arc auroral emission was observed to fade strongly for several hours
- This may have been attributable to reduced plasma flow shear during a prolonged solar wind rarefaction
- An isolated auroral spot emission is evidence of dayside reconnection at an expanded magnetosphere

Correspondence to:
J. Kinrade,
j.kinrade@lancaster.ac.uk

Citation:
Kinrade, J., et al. (2017), An isolated, bright cusp aurora at Saturn, *J. Geophys. Res. Space Physics*, *122*, 6121–6138, doi:10.1002/2016JA023792.

Received 9 DEC 2016
Accepted 23 MAY 2017
Accepted article online 30 MAY 2017
Published online 13 JUN 2017

An isolated, bright cusp aurora at Saturn

J. Kinrade[1], S. V. Badman[1], E. J. Bunce[2], C. Tao[3], G. Provan[2], S. W. H. Cowley[2], A. Grocott[1], R. L. Gray[1], D. Grodent[4], T. Kimura[5], J. D. Nichols[2], C. S. Arridge[1], A. Radioti[4], J. T. Clarke[6], F. J. Crary[7], W. R. Pryor[8], H. Melin[2], K. H. Baines[9], and M. K. Dougherty[10]

[1]Department of Physics, Lancaster University, Lancaster, UK, [2]Department of Physics and Astronomy, University of Leicester, Leicester, UK, [3]Space Environment Laboratory, National Institute of Information and Communications Technology (NICT), Tokyo, Japan, [4]LPAP, Institut d'Astrophysique et de Géophysique, Université de Liège, Liège, Belgium, [5]RIKEN Nishina Center for Accelerator-Based Science, Saitama, Japan, [6]Department of Astronomy and Center for Space Physics, Boston University, Boston, Massachusetts, USA, [7]LASP, University of Colorado Boulder, Boulder, Colorado, USA, [8]Department of Science, Central Arizona College, Coolidge, Arizona, USA, [9]Jet Propulsion Laboratory, California Institute of Technology, Pasadena, California, USA, [10]Space and Atmospheric Physics Group, Blackett Laboratory, Imperial College London, London, UK

Abstract Saturn's dayside aurora displays a number of morphological features poleward of the main emission region. We present an unusual morphology captured by the Hubble Space Telescope on 14 June 2014 (day 165), where for 2 h, Saturn's FUV aurora faded almost entirely, with the exception of a distinct emission spot at high latitude. The spot remained fixed in local time between 10 and 15 LT and moved poleward to a minimum colatitude of ~4°. It was bright and persistent, displaying intensities of up to 49 kR over a lifetime of 2 h. Interestingly, the spot constituted the entirety of the northern auroral emission, with no emissions present at any other local time—including Saturn's characteristic dawn arc, the complete absence of which is rarely observed. Solar wind parameters from propagation models, together with a Cassini magnetopause crossing and solar wind encounter, indicate that Saturn's magnetosphere was likely to have been embedded in a rarefaction region, resulting in an expanded magnetosphere configuration during the interval. We infer that the spot was sustained by reconnection either poleward of the cusp or at low latitudes under a strong component of interplanetary magnetic field transverse to the solar wind flow. The subsequent poleward motion could then arise from either reconfiguration of successive open field lines across the polar cap or convection of newly opened field lines. We also consider the possible modulation of the feature by planetary period rotating current systems.

1. Introduction

Detections of dayside reconnection signatures at Saturn provide evidence of the solar wind influence on magnetospheric and ionospheric dynamics. Auroral imagery offers a valuable way of remotely detecting the occurrence of reconnection.

Earth's dayside auroral morphology has a well-studied response to the solar wind interaction [e.g., *Milan et al.*, 2010] and Dungey circulation [*Dungey*, 1961] circulation of the magnetosphere. Low-latitude reconnection between a southward interplanetary magnetic field (IMF) and planetary field at the dayside magnetopause, resulting in open flux production, generates a cusp spot just equatorward of the open-closed field line boundary (OCB) and poleward moving forms [e.g., *Milan et al.*, 2000a]. Reconnection at high latitudes between a northward IMF and the open lobe field lines generates an auroral spot just poleward of the OCB and equatorward moving arcs [e.g., *Øieroset et al.*, 1997; *Milan et al.*, 2000b; *Frey et al.*, 2002]. Signatures of high-latitude dayside reconnection and cusp precipitation in the terrestrial aurora are correlated with solar wind density (affecting emission intensity) and the transverse IMF component (controlling local time position) [e.g., *Milan et al.*, 2000b; *Frey et al.*, 2002; *Fuselier et al.*, 2002; *Fear et al.*, 2015].

Saturn's auroras, however, are the product of a highly rotational magnetosphere, displaying clear responses to both the solar wind [e.g., *Clarke et al.*, 2005, 2009; *Crary et al.*, 2005] and internal plasma sources [e.g., *Mitchell et al.*, 2009]. The main auroral emission is driven by flow shears in the outer magnetosphere, initially thought to map to an upward current region near the OCB [e.g., *Cowley et al.*, 2004; *Bunce et al.*, 2008]. Subsequent detailed studies have shown that the maximum upward field-aligned currents (FAC) map to a

region 1–2° equatorward of the OCB, suggesting an additional dependence on the ionospheric conductivity [e.g., *Talboys et al*., 2009; *Jinks et al*., 2014; *Hunt et al*., 2014]. A persistent dawn arc shows little dependence on IMF direction [*Meredith et al*., 2014] in comparison to the strong auroral modulation by the IMF observed at Earth [e.g., *Milan et al*., 2010]. Mapping to the outer ring current region [*Belenkaya et al*., 2014], the dawn arc has been observed to expand and brighten in response to tail reconnection events [*Mitchell et al*., 2009; *Nichols et al*., 2014; *Radioti et al*., 2014, 2016; *Badman et al*., 2016] and hot plasma injections in the absence of solar wind triggering [e.g., *Gérard et al*., 2006]. Absence of the dawn arc has only occasionally been observed [e.g., *Nichols et al*., 2016].

Spiral forms encircling the entire auroral region have been observed in response to solar wind compression dynamics [e.g., *Clarke et al*., 2005; *Cowley et al*., 2005]. *Grodent et al*. [2005] reported subcorotating auroral features at Saturn during quiet solar wind conditions, when an emission spot was observed to decelerate in angular velocity from 70% to 20% of corotation as it moved past noon, reducing in brightness and moving rapidly poleward by ~10° at the same time. This feature rotated from dawn before this point, and similar features have been interpreted as signatures of nightside plasma injection [*Cowley et al*., 2005; *Lamy et al*., 2013; *Nichols et al*., 2014] or propagating ULF waves [*Meredith et al*., 2013].

The efficiency of magnetopause reconnection at Saturn has been questioned because of the different plasma environments and velocity flow shear on either side of the magnetopause compared to the Earth [e.g., *Masters et al*., 2012; *Desroche et al*., 2013]. However, various auroral and in situ signatures of reconnection have been identified. Low-latitude reconnection signatures in Saturn's auroras appear as intensifications within the main emission in the noon-dusk region that subsequently bifurcate poleward [*Radioti et al*., 2011; *Badman et al*., 2013; *Jasinski et al*., 2014]. These bifurcations are sometimes observed to pulse in intensity with an ~1 h period and have poleward speeds of ~2°/h [*Radioti et al*., 2013; *Mitchell et al*., 2016; *Nichols et al*., 2016]. There is some evidence that these auroral bifurcations are more likely to occur when the magnetosphere is compressed [*Badman et al*., 2013]. Simultaneous Hubble Space Telescope (HST) observations and Cassini measurements of the upstream solar wind revealed that Saturn's dayside auroras have a dependency on IMF polarity [*Meredith et al*., 2014], with patchy postnoon emissions (possibly bifurcations not resolved by HST) visible during periods of positive B_Z but absent during negative B_Z; Saturn's magnetic dipole has opposite direction to Earth's.

In addition to auroral observations, in situ Cassini measurements of heated magnetosheath plasma, a component of the magnetic field normal to the magnetopause [*McAndrews et al*., 2008], and escaping magnetospheric electrons [*Badman et al*., 2013] have indicated reconnection activity at the low-latitude magnetopause. Magnetosheath plasma has been identified in Saturn's magnetospheric cusps, including stepped ion dispersion signatures indicating bursty reconnection [*Jasinski et al*., 2014; *Arridge et al*., 2016]. *Jasinski et al*. [2016] have identified a dayside flux transfer event, confirming that Saturn's magnetopause is conducive to multiple reconnection sites and open flux generation.

High-latitude (i.e., poleward of the cusp) reconnection signatures, reminiscent of those seen under northward IMF conditions at Earth, have also been observed [*Gérard et al*., 2005; *Badman et al*., 2013; *Mitchell et al*., 2016; *Palmaerts et al*., 2016]. *Gérard et al*. [2005] investigated a cusp spot signature fixed at noon local time for at least 30 min during an interval of intermediate IMF strength following a minor compression of the solar wind. These observations were generally consistent with the model of *Bunce et al*. [2005], which estimates reconnection-driven flows and resulting polar cusp UV auroral emissions for different IMF conditions. *Meredith et al*. [2014] observed a high-latitude, prenoon emission signature during a period of upstream southward IMF, extending from the main dawn arc emission to the spin pole itself. This case was attributed to lobe reconnection, consistent with the high latitude of the emission and the expected location of the magnetopause reconnection site during southward IMF at Saturn.

In addition to these solar wind-driven signatures, Saturn's auroral emissions also display a rotational modulation in intensity and location. Based on observations of near-planetary period oscillations (PPO) in the magnetic field, this modulation is attributed to a system of FACs rotating independently, and with slightly different periods, in the northern and southern hemispheres [e.g., *Provan et al*., 2009, 2016; *Andrews et al*., 2010; *Hunt et al*., 2014, 2015]. Auroral emission intensity increases where the rotating FAC system is directed upward (implying downward precipitating electrons) [e.g., *Badman et al*., 2012]. The intensity of the dawn arc is modulated by PPO phase in the southern hemisphere, but this variation is not as clear in the northern

hemisphere [*Nichols et al*., 2010, 2016]. The additional magnetic field component of the PPO perturbations effectively tilts Saturn's background field, and the entire oval oscillates by up to several degrees of latitude with the PPO phase [*Nichols et al*., 2008, 2010, 2016].

The paucity of studies combining auroral imagery, Cassini magnetopause encounters, and reliable upstream solar wind monitoring at Saturn means that further observations are required to understand the dayside reconnection processes and their role in driving auroral currents and plasma flows. In this case study we report on Hubble Space Telescope (HST) observations of Saturn's northern FUV auroras on 14 June 2014, together with in situ Cassini measurements of the upstream solar wind conditions and magnetopause location. Observations from three consecutive HST orbits on this day revealed a period of unusually quiet emission morphology, with the exception of an isolated, bright poleward signature that persisted for several hours on the dayside. Here we investigate the potential drivers of the auroral emission in the context of dayside reconnection under expanded magnetospheric conditions. We also discuss the possible modulation of the auroral signature by the rotating planetary-period current system.

2. Data

2.1. HST STIS Pipeline

The HST Space Telescope Imaging Spectrograph (STIS) captured the images used in this study, during three HST orbits on 14 June 2014 (day 165). The instrument's SrF2 filter excludes hydrogen Lyman alpha emission at 121.6 nm but passes the H_2 Lyman and Werner bands in the range 125–190 nm. Systematic image processing followed the pipeline steps developed by Boston University [*Clarke et al*., 2009; *Nichols et al*., 2009], including flat-fielding, dark count subtraction and correction for geometric distortion. Emissions from the planetary disk and geocorona were also removed using the same method as *Clarke et al*. [2009], i.e., determining best fit Minnaert coefficients for the center-to-limb variation and using a latitudinal intensity profile extrapolated over the auroral region. Close to the auroral region the uncertainty in the empirically derived background is ~2–3 kR. The images were scaled to a standard distance between HST and Saturn of ~8.2 AU and projected onto a 0.25° × 0.25° planetocentric latitude and longitude grid at an emission altitude of 1100 km above the 1 bar pressure level [*Gérard et al*., 2009]. The STIS MAMA detector consists of 1024 × 1024 pixels, with a single pixel dimension of 0.025 arc sec; this translates to a range of distances subtended by a single pixel projected on the planet surface, but at nadir this is ~476 km with an Earth-Saturn distance of 8.2 AU and taking account of the ~0.08 arc sec point spread function. Spatial uncertainties in the images arise, however, from determination of the planet center and distortion of projected pixels toward the limb; *Grodent et al*. [2003] showed that this spatial uncertainty is ~1° for typical observation geometries (~1000 km on the planet surface).

Exposure times ranged between ~700 and 840 s. Photon count rates were converted to intensity values of unabsorbed H_2 emission across the wavelength range 70–180 nm using the conversion factor of 1 kR = 3994 counts per second given by *Gustin et al*. [2012], assuming a color ratio of 1.1 across Saturn's auroral region.

2.2. Upstream Solar Wind Conditions

The Cassini spacecraft entered the solar wind on day 160 for several hours, with the magnetometer (MAG) [*Dougherty et al*., 2004] instrument providing measurement of the IMF conditions upstream of Saturn (5 days prior to the auroral observations). Plasma measurements from the CAPS instrument were not available during the study period. Magnetic field measurements and spacecraft position are given in kronocentric solar magnetospheric (KSM) coordinates, which have Saturn at the origin; the *X* axis is directed toward the Sun, *Z* is defined such that Saturn's rotation and magnetic axis lies in the *XZ* plane, and *Y* lies in Saturn's rotation and magnetic equatorial plane [*Dougherty et al*., 2005]. The solar wind encounter was identified by the sharp decrease in IMF magnitude as Cassini left the magnetosheath. We used this period to verify the validity of the solar wind projection models described below. Several days later, between days 163 and 164, Cassini crossed the magnetopause boundary inbound, followed by an excursion back into the magnetosheath before reentering the magnetosphere. We used the position of Cassini at these crossing times to estimate the dynamic pressure and subsolar standoff distance of the magnetopause, using the *Kanani et al*. [2010] magnetopause model.

In addition to the in situ Cassini measurements, we used projections from two 1-D-MHD propagation models to gauge incident solar wind conditions during the HST observation period. Both the Michigan Solar Wind Model (mSWiM) [*Zeiger and Hansen*, 2008] and *Tao et al.* [2005] models project multispacecraft measurements at 1 AU provided by the OMNIweb service, using the source satellite that is closest to opposition with the desired target. Conditions for projection are optimal at opposition, when the actual boundary conditions at 1 AU are propagated, including transient signatures like shock fronts. Day 165 of 2014 was within 4 days of apparent Earth-Saturn opposition (actual opposition plus approximate solar wind travel time to Saturn) on day 161. Solar wind velocity is the most accurately modeled parameter (based on correlation with 12 years of in situ measurements from the Voyager, Pioneer and Ulysses missions [*Zeiger and Hansen*, 2008]), followed by IMF magnitude, number density, and transverse field components. Accurate estimation of the IMF B_Z component is not possible with single-dimension MHD solar wind models. Dynamic pressure, P_{DYN}, was obtained by converting the number density to a mass density, ρ, and then multiplying by the summed-squared velocity components ($P_{DYN} = \rho v^2$). The input data availability from OMNIweb was ~97% for 2014, and the solar wind speed recurrence index (a measure of solar wind speed consistency between successive solar rotations) was low (0.17) during essentially the maximum period of the solar cycle—both of these factors are important for reliable solar wind prediction at 10 AU, the outer boundary of the models. The impact of low solar wind speed recurrence on the model's prediction efficiency is minimal during apparent opposition; however, we added a conservative ±40 h uncertainty window to the solar wind parameters [see *Zeiger and Hansen*, 2008, Figure 11].

3. Observations

3.1. Solar Wind Models

Both solar wind projection models indicate a gradual decrease in velocity over the 2 weeks prior to the observation window (blue vertical line in Figure 1), from ~420 km s^{-1} to below 350 km s^{-1}. The magnitude of the IMF, $|B|$, was also low throughout this period (< 0.1 nT), with the exception of a small increase to ~0.2 nT on day 167 (the end of the uncertainty window shown by the gray shaded region in Figure 1). The trend in dynamic pressure was similar, being between 0.001 and 0.005 nPa until an apparent region of solar wind disturbance beginning on day 167 that persisted for a week afterward.

Finally, the transverse B_T component was positive (~0.1 nT) for an extended period including the observation window. Generally, the estimated parameters are similar in both projection models and consistent with a period of rarefaction at Saturn preceding the HST observation window on day 165; we discuss this further in section 4.1. In the next section we compare these projected magnetic parameters with IMF measurements from Cassini during a brief solar wind encounter on day 160.

A wider picture of the solar wind activity from projections over April, May, and June 2014 (not shown here) indicated that the period of disturbance between days 167 and 175 (see Figure 1) may have originated from a mix of corotating interaction region and interplanetary coronal mass ejection-like structuring recorded at 1 AU around days 120–121 of 2014. Prior to this disturbance, the solar wind velocity appears to have been remarkably low for ~1 month, falling to below 300 km s^{-1} at times and approaching the slowest solar wind speeds encountered at 1 AU [*Sanchez-Diaz et al.*, 2016]. It is possible that this case study captures an auroral morphology at Saturn during a prolonged period of extremely quiet ambient solar wind.

3.2. In Situ Cassini Measurements

We examine in situ Cassini magnetometer measurements to determine both upstream conditions in the solar wind and how compressed the magnetosphere was. Prior to the HST observations, from day 160 onward, Cassini's orbit was inbound, crossing the equatorial plane close to local noon on day 164. Cassini's trajectory (KSM coordinates) during revolution 205 is shown in Figure 2, with annotation showing the spacecraft location at the time of HST observations on day 165 (red dot). Figure 2a shows the orbital trace (solid black line) as viewed from above the northern hemisphere in the KSM *X-Y* plane and Figure 2b as viewed from the dawn flank in the KSM *X-Z* plane. The Sun is to the right of the figure in each case. Black dots show Cassini's position on the days annotated. Further annotation is based on Cassini MAG measurements discussed below (see Figure 3), namely, a solar wind encounter on day 160 (green dot) and several magnetopause crossings on days 163–164 (blue dots). For reference and based on these crossings, two magnetopause positions are

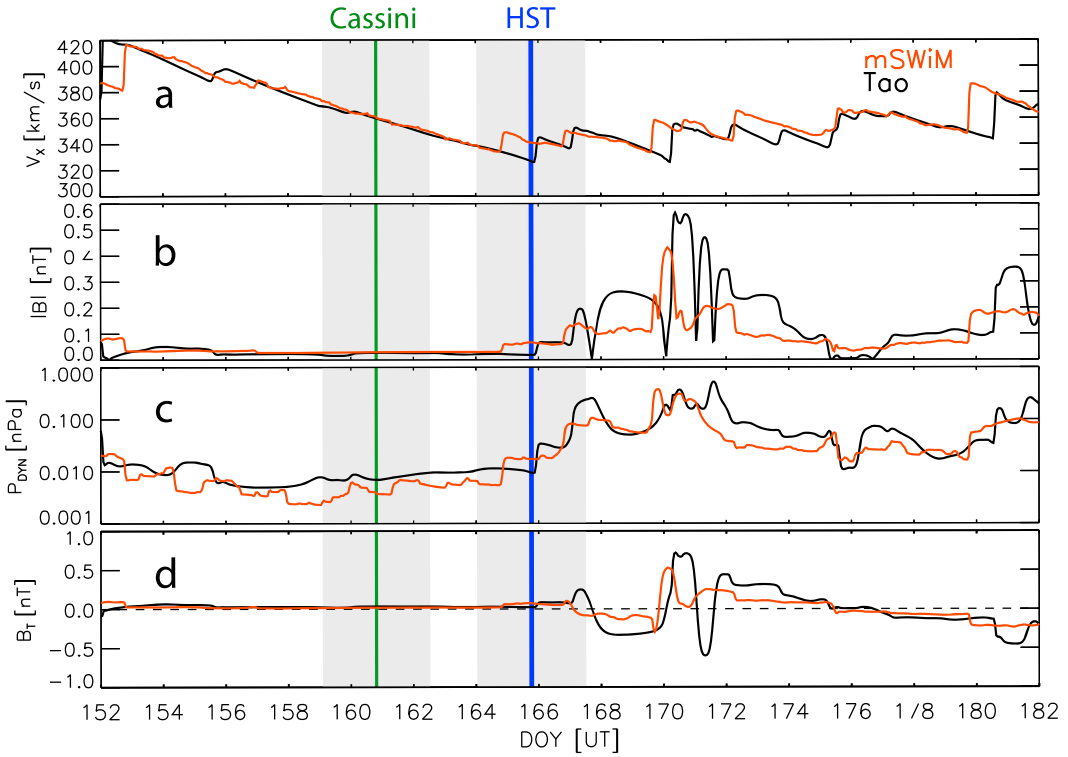

Figure 1. Solar wind parameters throughout June 2014, as projected using two different 1-D MHD models. mSWiM parameters [*Zeiger and Hansen*, 2008] are plotted in red and those from the *Tao et al.* [2005] model in black. (a) The component of solar wind velocity directed radially outward from the Sun, V_X, (b) IMF magnitude, (c) dynamic pressure (logarithmic scale), and (d) transverse IMF component in the radial-tangential-normal (RTN) frame (positive $B_T \approx$ negative B_Y in the KSM frame). For reference the blue vertical line marks the extent of the HST imaging window on day 165, and the green line marks the ~2 h time window of solar wind measurement made by Cassini on day 160 (see section 3.2). The two gray shaded regions represent conservative ±40 h uncertainty windows for the model projections; i.e., model parameters within the blue or green shaded times could take any value within the respective gray shaded uncertainty region.

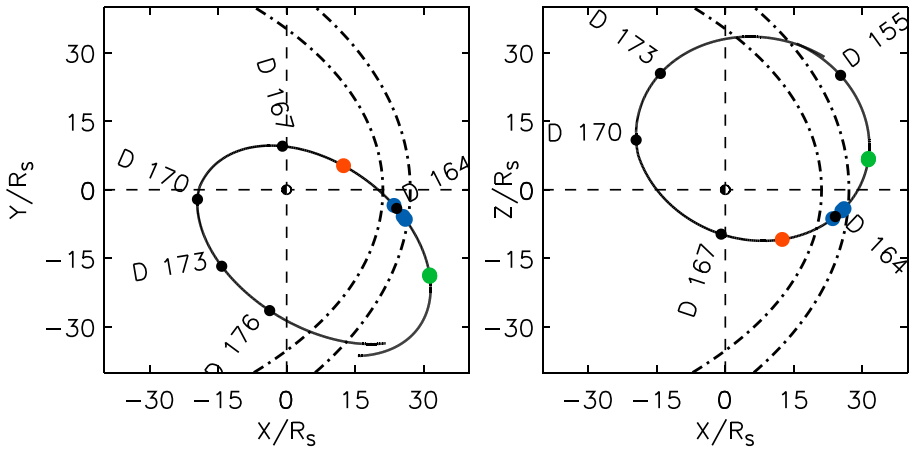

Figure 2. Cassini's trajectory during revolution 205 (days 151–184). (left) The spacecraft's orbital trace (solid black line) as viewed from above the northern hemisphere in the KSM *X-Y* plane. (right) The orbit trace as viewed from the dawn flank in the KSM *X-Z* plane. The Sun is to the right in each case. The green dot on the trajectory marks Cassini's position during a solar wind excursion identified in the MAG instrument data on day 160 (see Figure 3). The blue dots show magnetopause crossings also detected in MAG data on days 163–164. The red dot shows the spacecraft location at the time of the HST observations on day 165, and the black dots show spacecraft location at the beginning of the days annotated. Dash-dotted lines mark the magnetopause from the *Kanani et al.* [2010] model at standoff distances of 24 and 27 R_S.

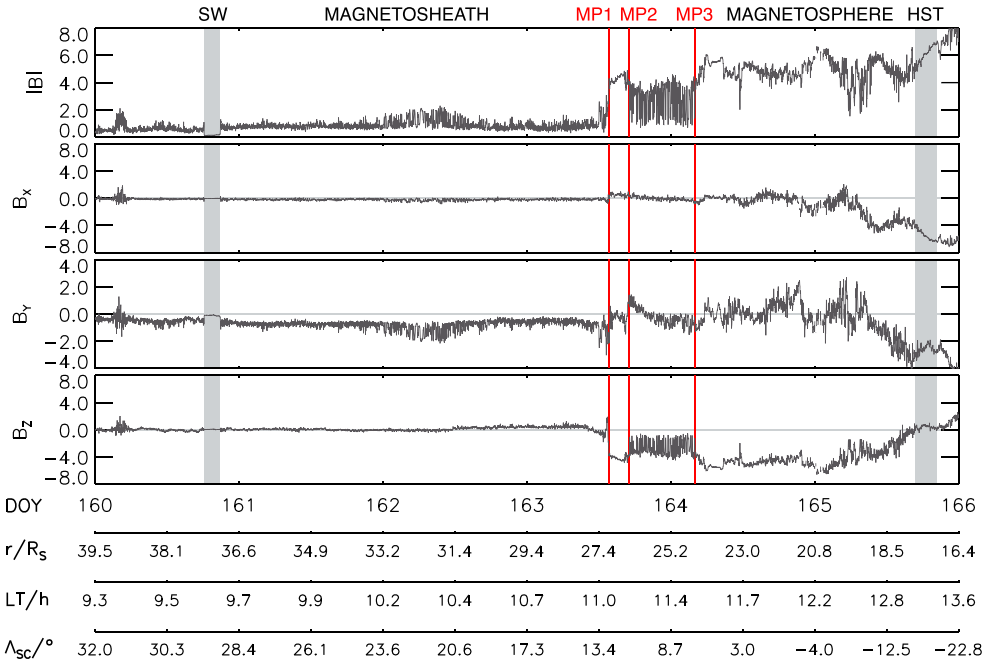

Figure 3. Cassini KSM magnetometer data during days 160–165 of 2014. All *y* axes have units of nanotesla. A solar wind encounter was evident during ~1814–2038 UT (shaded gray) on day 160 as a reduction in $|B|$, labeled SW. Inbound magnetopause crossings are visible at ~1341 UT on day 163 (red vertical line, labeled MP1) and ~0405 UT on day 164 (red line, MP3), with a reentry into the sheath between these two times (MP2). Cassini planet center distance (R_S), local time (LT) position, and sub-Cassini latitude (Λ_{SC}) are provided in the additional axes. The HST imaging window on day 165 is also shaded gray and labeled HST.

shown in Figure 2 at standoff distances of 24 R_S and 27 R_S (dash-dotted lines), obtained using the *Kanani et al.* [2010] magnetopause model with Cassini's KSM position at the crossing times discussed below (see Figure 3 and Table 1).

Figure 3 shows Cassini MAG traces between days 160 and 166. The spacecraft's radial distance from planet center (r), local time (LT), and subsatellite latitude of the spacecraft (Λ_{SC}) are provided as additional axes. A solar wind encounter was evident as a reduction in $|B|$ on day 160 during ~1814–2038 UT (Cassini's position at this time is marked by the green dot in Figure 2). The IMF magnitude was ~0.1–0.15 nT, slightly above the ~0.05 nT level estimated by models at the same time, but this confirms the persistent low level in the wider context of the model traces (see Figure 1). The transverse B_Y component was consistently negative and ranged between −0.15 and −0.1 nT, equivalent to the positive B_T component estimated by the model (also of similar magnitude). The Cassini MAG instrument also provides a measure of B_Z component, which ranged from 0.0 to 0.1 nT during the solar wind sample; there is no accurate estimate of this parameter from the projection models for comparison. The magnetic measurements from Cassini's solar wind encounter verify the projected models for several hours on day 160. The direction of the IMF is also preserved in the magnetosheath, and Figure 3 shows that the IMF B_Y component was consistently negative between the solar wind

Table 1. Latitude Local Time (LT) Extents and Power of the Auroral Spot[a]

Image Start Time (UT)	Maximum Colatitude (deg)	Minimum Colatitude (deg)	LT Minimum (h)	LT Maximum (h)	Power (GW)
16:40	13.0	6.8	11.5	14.7	1.87
17:12[a]	12.5	8.0	11.2	14.4	1.12
18:08	12.0	6.3	11.3	15.3	2.69
18:43	10.8	5.3	10.0	15.4	3.13
19:44	8.5	4.8	12.2	15.3	0.86
20:18	8.3	4.3	10.6	14.6	0.73

[a]Combined properties of the two dark gray regions around noon at 1712 UT in Figure 5a, considered to be part of the same spot feature here and separated only as a result of the systematic image threshold used to track the features.

encounter on day 160 up to the magnetopause crossing on day 163. The B_Z component measured in the sheath was mostly positive (up to ~1.0 nT) on day 163, before reversing polarity to ~ −1.0 nT just before the magnetopause crossing. It is reasonable to suggest that solar wind conditions varied little in the days following the solar wind encounter up to the HST observation period (with the exception of IMF B_Z polarity), given the wider picture of an apparently stable rarefaction period. Model conditions were also optimum at the time in terms of object opposition and data coverage (see section 2.2). Saturn kilometric radio (SKR) emissions measured by the Cassini Radio and Plasma Wave Science (RPWS) investigation were extremely low throughout days 160–166 (not shown here), although we note the presence of a single low-power, low-frequency extension (LFE) on day 162. Strong LFE signatures have been linked with the arrival of solar wind compressions at Saturn [*Badman et al*., 2008] and in this case may be associated with the period of magnetosheath field fluctuations of several nanotesla on day 162 (see Figure 3). This was possibly a short-lived compression region not resolved by the projection models.

Closer to the HST observation window, Cassini crossed the magnetopause inbound at 1341 UT on day 163 (marked "MP1" in Figure 3). This is evident in Figure 3 as an increase in $|B|$, from magnetosheath fluctuations below ~2 nT prior to the crossing to values of ~4–6 nT. Cassini appeared to reenter the magnetosheath between ~1700 and 0500 UT indicated by the rapid fluctuations of several nanotesla; these "dips" in magnitude are suggestive of mirror mode instability structures observed mostly in low-β plasma near the magnetopause and on the flanks [*Cattaneo et al*., 1998; *Joy et al*., 2006]. This outbound magnetopause crossing, marked "MP2" in Figure 3 (also red vertical line), suggests that the magnetopause was compressed beyond the spacecraft before Cassini eventually entered the magnetosphere again at 0405 UT on day 164 ("MP3"). We used the magnetopause model of *Kanani et al*. [2010] (see description in section 2.2) to produce subsolar magnetopause standoff distances, R_{MP}, of ~24–27 R_S for these two inbound crossings.

A magnetopause standoff distance of ~27 R_S corresponds to an expanded state of the magnetosphere according to the apparent bimodal distribution of standoff distance identified by *Achilleos et al*. [2008] and more recently by *Pilkington et al*. [2015], the other state being "compressed" with values of ~21 R_S. The range we find therefore, of ~24–27 R_S, indicates that the magnetosphere was closer to a state of expansion just a day before the HST observation window. The protracted magnetopause crossing may be attributable to a modest compression of an expanded magnetosphere. The corresponding range of solar wind dynamic pressure from the *Kanani et al*. [2010] model for each potential magnetopause crossing was 0.0086–0.0143 nPa, compared with the solar wind propagation model values of 0.0017–0.0022 nPa at the same time. We discuss this further in section 4.1.

3.3. HST STIS Images

Figure 4 shows a sequence of six HST STIS images of Saturn's northern auroral region, captured on three HST orbits between 1755 and 2148 UT on day 165; together, they form the main focal point of this study. Labeled underneath Figures 4a–4f are both the HST exposure time stamp (start-end time) and light travel-corrected time stamp at Saturn ("SAT UT"), ranging from 1755 to 2148 UT and 1640 to 2032 UT, respectively. The images are stereographic projections produced using the pipeline summarized in section 2.1 and are rotated such that local noon is at the bottom of each image, with dawn to the left and dusk to the right. The black area at the top of each image (nightside) is the result of cropping out distorted pixels at the far limb following projection onto the spheroid. A sub-Earth latitude of ~22° subtended at Saturn allowed HST to observe the main auroral emission latitudes across the whole local time range, including the nightside region as Saturn enters its northern spring season. Based on the latest model values from *Provan et al*. [2016], the expected local time angle of the maximum upward FAC associated with the northern PPO rotating current system is shown by white plus symbols (6 h behind the northern PPO dipole). White dash symbols show the expected local time angle of the maximum downward FAC associated with the northern PPO systems. White dashed lines show the local time angle of the northern effective dipole. The pink trace on Figure 4a marks the ionospheric footprint of Cassini during day 165, mapped using the *Burton et al*. [2010] planetary field model, modified by a ring current contribution for an expanded magnetosphere with standoff distance of 26 R_S [*Bunce et al*., 2008]; this model does not include effects from the magnetopause or tail currents and therefore is most accurate sufficiently inside the magnetopause (within ~15–16 R_S). Figure 3 shows that Cassini was located in the IMF and magnetosheath prior to approximately midday on day 163; hence, we use the *Bunce et al*. [2008] model to approximate Cassini's footprint on day 165 only.

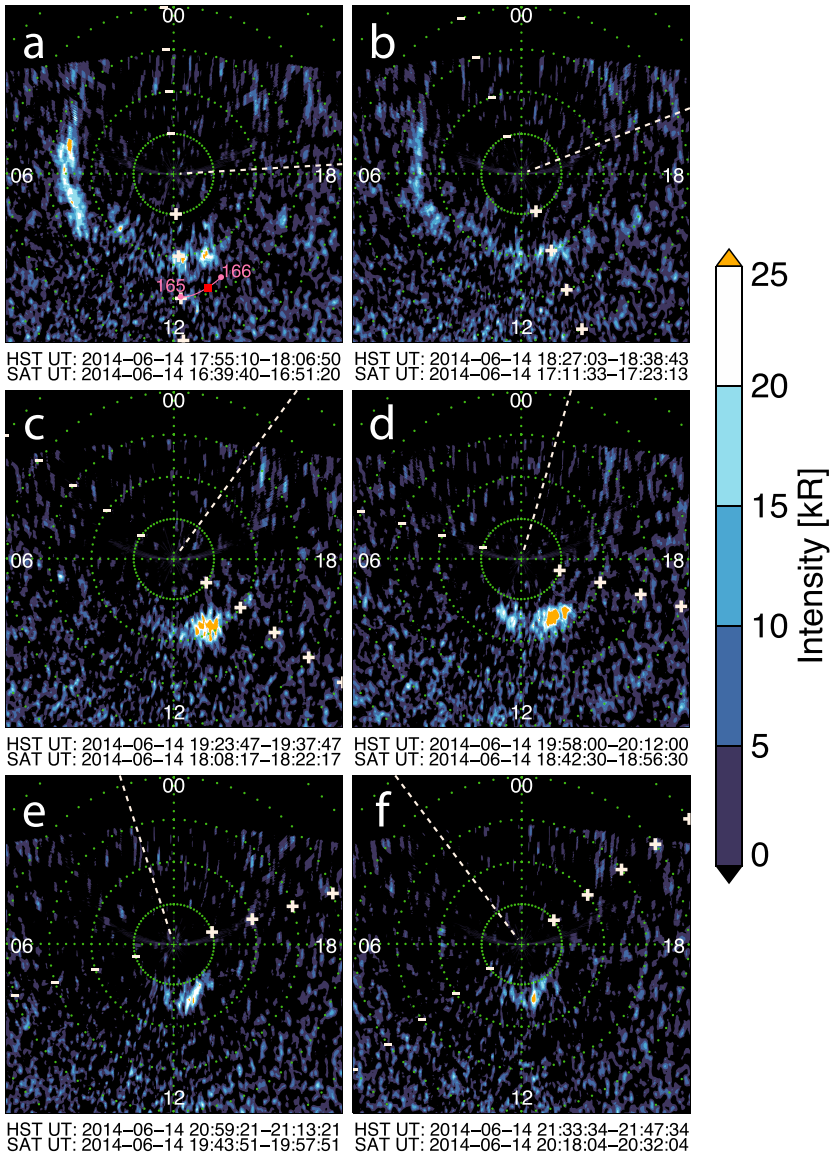

Figure 4. (a–f) A sequence of HST STIS images of Saturn's northern FUV aurora (SrF2 filtered) in stereographic projection. Local noon is fixed at the bottom of each image. The sequence spans times 16:39:40 to 20:32:04 Saturn UT on day 165 of 2014. Time between images varies, with image start and end times labeled under each exposure in HST UT and light travel time-corrected time at Saturn, labeled SAT UT. Green dots show points of 1° latitude at intervals of 90° longitude and points of 5° grid longitude at intervals of 5° latitude from the pole. White dashed lines mark the local time position of the model *Provan et al.* [2016] northern PPO current system effective dipole, with associated maximum upward and downward current regions shown as plus and minus symbols. The pink trace in Figure 4a shows Cassini's ionospheric footprint on day 165, as described in the text. The red square marks Cassini's footprint at the midexposure time in Figure 4a.

The earliest image in the sequence, Figure 4a (1640–1651 Saturn UT), shows an auroral morphology with two main features. A dawn arc emission extended between ~3 and 9 local time (LT) with colatitude extent of ~5–11° and intensities of up to ~30 kR. Also visible is an area of emission located between ~9 and 13° colatitude and ~11–14 LT. This area possibly consisted of two separate spot structures separated in local time by only tens of minutes (two orange spots near noon in Figure 4a), but in the presence of image noise and with a lack of prior imagery to observe temporal development, this is unclear. The morphology in Figure 4a persisted in Figure 4b (1712–1723 Saturn UT) but with a marked decrease in intensity of both dawn arc and postnoon emissions to levels below ~20 kR. The dawn arc remained fixed in terms of colatitude at ~13°, but its latitudinal width decreased by several degrees, extending between ~9 and 13° (see extents of

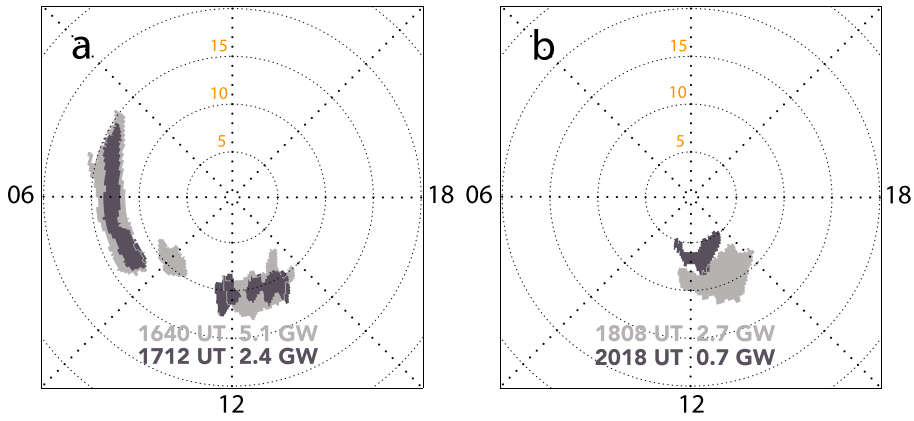

Figure 5. Auroral morphology at different times throughout the HST imaging sequence on day 165, in fixed local time, polar stereographic projection of Saturn's northern hemisphere. Degrees of colatitude are labeled in orange and marked by 1° black dots at intervals of 45° grid longitude. (a and b) In each window, the earlier morphology is shaded in light gray, the later in dark gray, with matching annotations of image exposure time and total emitted power at that time from all regions. Light gray lines outline the earlier morphology when structures overlap between exposures.

the dawn arc structure shown at 1712 UT in Figure 5a). The postnoon emission area faded to an intensity level just perceptible above the background but remained fixed in local time.

Figures 4c–4f clearly show a different morphology. The dawn arc emission, present in Figures 4a and 4b, had evidently faded to a level below the limit of detectability by ~1808 UT and remained absent throughout the rest of the observation window. Indeed, the only emissions detected in the rest of the sequence constituted an isolated spot feature fixed in local time around noon, which may have been a reappearance of the noon spots in the previous two images. Visible in each of Figures 4c–4f, the spot was brightest in Figure 4d (1843–1857 Saturn UT) with a peak intensity of 49 kR.

In order to track the spatial and temporal development of this feature (and that of the earlier dawn arc and noon emissions), we applied several image processing steps to systematically quantify the spot's area and intensity. A second motivation for this was to extract an estimate of emitted auroral power from the separate emission structures. The corresponding nonprojected images of those in Figure 4 were first smoothed using a seven-pixel boxcar average then regions of interest defined as the pixels where intensity is >3 kR. The total emitted power (see Table 2) was calculated as the multiple of total pixel count rate with the squared HST-Saturn distance (at the time of exposure) and a conversion factor of 9.04×10^{-10} [after *Gustin et al.*, 2012].

Results of the above procedure are shown by the two stereographic projections in Figure 5. The shaded areas represent the reprojected regions of interest identified by the tracking procedure. Figure 5a depicts the dawn arc and postnoon emission morphology in Figure 4a (1640 UT, light gray) and Figure 4b (1712 UT, dark gray). Figure 5b depicts the extents of the isolated spot feature of Figure 4c (1808 UT, light gray) and Figure 4f (2018 UT, dark gray), i.e., the earliest and latest images in which the spot constituted Saturn's entire auroral emission in Figure 4. The total auroral power emitted at each time is annotated in the matching gray shade. We omit the 1842 UT (Figure 4d) and 1943 UT (Figure 4e) morphologies in Figure 5b for clarity, but area extents and power values of the isolated spot are listed in Table 1.

Together, Figure 5 and Table 1 quantify the basic development of the auroral morphology and power output during the HST observation window. We note that the simple image processing steps here may not be as effective in the tracking and separation of more complex auroral structure at Saturn. Figure 5a clearly shows narrowing of the dawn arc between the two earlier images, together with the patches of emission around noon that remain approximately fixed in local time and colatitude. The smaller patch of emission at 1640 UT, located poleward of the dawn arc at ~8–10 LT and 8–11°, was detected in only one exposure (Figure 4a), nevertheless contributing to the total emitted power of the aurora (above the detection threshold) at that time. The estimated total auroral power output reduced by a factor of ~2, from 5.1 GW to 2.4 GW, in ~30 min between exposures. Looking at Figure 5b, we can see that, following the disappearance of the

Table 2. Auroral Cusp Spot Parameters From the Model of *Bunce et al.* [2005], the Adapted Model Results and Observations of *Gérard et al.* [2005] and the Brightest Spot in This Study

Study	Reconnection Location	Area (m^2)	$<I>$ (kR)	I_{MAX} (kR)	Power (GW)	Power per Unit Area (GW/10^{12} m^2)
Bunce et al. [2005]	High latitude	0.3×10^{12}	11.2	41.0	0.00–0.17	0.00–0.55
Bunce et al. [2005]	Low latitude	2.1×10^{12}	25.6	193.9	0.07–1.10	0.03–0.52
Gérard et al. [2005]	High latitude	8.0×10^{12}	0.7–25.4 (21.0)[a]	-	0.06–2.20 (5.0)[a]	0.00–0.28 (0.63)[a]
Gérard et al. [2005]	Low latitude	6.0×10^{12}	18.4–105.5 (20.0)[a]	-	1.3–7.6 (2.5)[a]	0.22–1.27 (0.42)[a]
This study	?	1.6×10^{12}	11.1	49.0	0.73–3.13	0.46–1.96

[a]HST observed parameters from the *Gérard et al.* [2005] study.

dawn arc, the now isolated spot moved poleward while remaining fixed at ~10–15 LT (noting that a small area at high latitude spans a wide local time range). Its estimated power output decreased from 2.7 GW to 0.7 GW over ~ 2 h. It is interesting to note that the 2.7 GW power output of the isolated spot at 1808 UT was greater than the 2.4 GW emitted by the combined auroral forms at 1712 UT.

Table 1 provides the maximum spatial extents of the isolated spot in each exposure of Figure 4, based on the areas identified through image processing and reprojection to a stereographic grid. After 1808 UT the spot generally reduced in both area and emission power as it moved poleward (this is discussed further in section 4).

4. Discussion

We now consider the cause of the unusual auroral morphology observed by HST on day 165, the fading and eventual absence of the dawn arc and an isolated spot moving to high latitude.

4.1. Solar Wind Conditions and State of Magnetosphere

Our interpretation of Saturn's northern auroral morphology on day 165 depends on the state of both the magnetosphere and incoming solar wind. The solar wind projection models (section 3.1), complimented by Cassini measurements (section 3.2), indicate that the HST observations were made following a prolonged period of rarefaction. For 2 weeks (days 153–165) the radial velocity gradually decreased to below 350 km s^{-1}, and the IMF magnitude was consistently $<$0.1 nT, in agreement with statistical values associated with rarefaction regions at Saturn [*Jackman et al.*, 2004]. On 2 days prior to the HST observations, estimates of dynamic pressure from the solar wind models (Figure 1) and *Kanani et al.* [2010] model during detected magnetopause crossings (Figure 3) were similarly low, with maximum values of 0.0022 nPa and 0.0143 nPa, respectively. The solar wind propagation models also show a period of disturbance developing after day 167 (toward the end of the uncertainty window in Figure 1), and it is possible that the auroral images were taken during the early stages of a compression in the solar wind, in which the projected IMF magnitude and dynamic pressure increased to ~0.2 nT and 0.25 nPa, respectively. However, the images show no evidence of the "storm" time morphology associated with strong magnetospheric compression (as reviewed by *Meredith et al.* [2015]), and we conclude that the auroras observed do not correspond to any significant compression interval.

Based on the two magnetopause crossings of Cassini identified in Figure 3, estimates of the subsolar standoff distance were obtained using the *Kanani et al.* [2010] magnetopause surface model (Table 1). Cassini was well positioned to enable this estimate, having crossed the magnetopause close to local noon and at low latitude just the day before the HST observations (see blue dots in the trajectory plots of Figure 2). The estimated standoff distance reduced from ~27 R_S to ~24 R_S in the ~14.5 h between resampling the magnetopause, suggesting compression of the magnetosphere beyond the spacecraft during this time. Although the solar wind projections show no evidence of compression transients, the Cassini MAG trace did detect minor fluctuations of the magnetosheath field magnitude on day 162 (Figure 3) associated with a possible low-frequency extension in SKR emission. These standoff distance estimates do, however, fall into the expanded or "inflated" end of the bimodal standoff distribution identified statistically by *Pilkington et al.* [2015], which peaks at ~27 R_S.

The strongest indication here of an expanded magnetosphere may be the complete disappearance of Saturn's dawn arc (Figures 4 and 5). A dawn arc is normally present to some degree in this highly

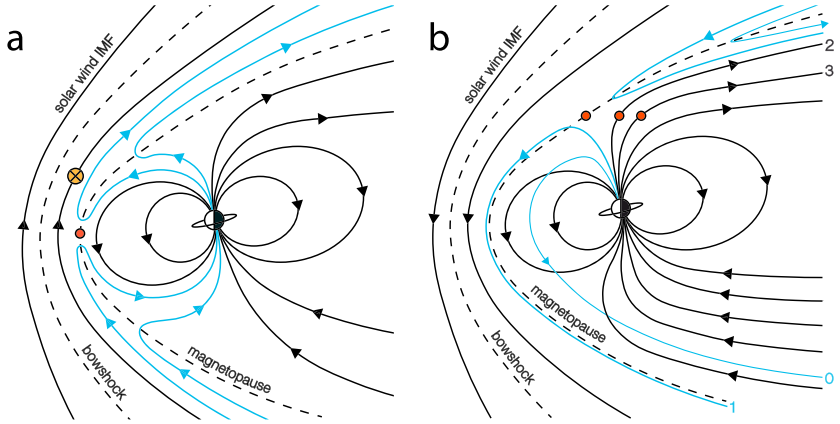

Figure 6. Conceptual sketches showing the dayside reconnection process at Saturn, as viewed in the day-night meridian with the Sun to the left in each case. Solid black lines with arrows represent solar wind and magnetospheric field orientation. Reconnection sites are shown by red dots, where the IMF and planetary field lines are antiparallel. Newly reconfigured field lines (following reconnection) are shaded blue. Black dashed lines mark the bow shock and magnetopause boundaries. (a) The low-latitude case when IMF is northward. The yellow circled cross indicates a negative B_Y component of the IMF as indicated by Cassini measurements and model projections in section 3. (b) The case of southward IMF, when draped solar wind flux may reconnect with planetary lobe flux. Field lines numbered 0–3 illustrate the circulation of newly reconfigured flux initially sunward (1) and then around the flanks with magnetosheath flow (0). Several reconnection sites are shown, indicating the successive reconnection with older, open lobe flux (2–3) required to produce poleward motion of an auroral signature.

rotational system, being driven by field-aligned currents (FACs) located equatorward of (and up to) the OCB, mapping to regions of flow shear or pressure gradients in the outer magnetosphere [*Jinks et al.*, 2014; *Belenkaya et al.*, 2014]. If the magnetosphere expands, the closed, outer field lines are expected to lag even further behind corotation as angular momentum is conserved, so that the shear in plasma angular velocity between these field lines and those at higher latitudes (including those possibly affected by solar wind viscous interactions in the magnetopause boundary layer or open field lines in the polar cap) is reduced on the dawnside. A complete switch off of Saturn's dawn arc further suggests that there is no sunward return flow along the dawn flank from nightside reconnection, which can enhance flow shears, pressure gradients, and hot plasma precipitation in this sector [*Cowley et al.*, 2005; *Grodent et al.*, 2005; *Mitchell et al.*, 2009; *Belenkaya et al.*, 2014; *Badman et al.*, 2016]. This scenario is quite feasible during a period of solar wind rarefaction; nevertheless, the complete absence of a dawn auroral arc has rarely been observed at Saturn, and in those cases dusk emissions were present instead [e.g., *Gérard et al.*, 2006; *Nichols et al.*, 2010, 2016].

4.2. Low-Latitude Dayside Reconnection

We now consider the possible dayside reconnection scenarios that may have produced the isolated auroral spot signature on day 165, considering its intensity, lack of motion in the corotation direction, and clear poleward motion throughout an observed lifetime of at least 2 h.

An auroral signature produced by dayside reconnection will appear initially at the OCB, regardless of whether the reconnection site is at low or high latitude. The spot observed here appeared at main emission latitudes before moving poleward. The first HST image at 1640 UT shows that the median colatitude of the noon emission was ~10°, compared with the ~13° of the dawn arc. This is consistent with the most recent HST survey of Saturn's northern auroral emissions by *Nichols et al.* [2016], which places the main emission between ~6.7°–12.5° colatitude at noon and ~13.4°–15.8° colatitude at dawn. The final image in the HST image at 2018 UT shows that the spot moved poleward and away from the main emission region to within 4.3° of the pole itself.

The poleward motion of the spot is consistent with precipitation on a newly opened field line following reconnection at low latitudes, under northward IMF conditions. As illustrated in Figure 6a, the magnetic tension and magnetosheath flow act to move newly opened field lines antisunward. *Meredith et al.* [2014] found significant noon-dusk sector auroral patch occurrence during northward IMF conditions (based on

HST images and Cassini solar wind measurements upstream). This matches the initial images of the HST sequence here, including the copresence of a dawn arc (present throughout the *Meredith et al*. [2014] study, although no clear dependence on IMF direction was found). The difference in this case is the fading and disappearance of the dawn arc after 1712 UT, simultaneous with the spot signature moving poleward and away from the main emission latitudes (compare Figures 5a and 5b).

Aside from the clear poleward motion of the spot, its position was also fixed in local time between ~10 and 15 LT (the center of the spot was fixed at ~1330 LT; see Table 1). If the dayside aurora were being driven by low-latitude reconnection, prior studies suggest that we may expect some evidence of subcorotation of auroral signatures or at least their equatorward extent [e.g., *Radioti et al*., 2013]. *Meredith et al*. [2014] report high-latitude emissions within the noon-dusk sector during northward IMF conditions that may be bifurcation structures at spatial scales not fully resolvable by the HST STIS. Bifurcations of the main emission region were observed more clearly by *Radioti et al*. [2011] and *Badman et al*. [2013] using the Cassini Ultraviolet Imaging Spectrograph and were associated with high dynamic pressure in the solar wind and subsequent magnetospheric compression. However, the solar wind appears to have been in rarefaction during day 165 (see section 4.1), and we see no evidence of rotation or bifurcation of the auroral emissions. Considering the polarity of Saturn's magnetospheric dipole and magnetic tension forces following reconnection with the IMF, a dawnward transverse IMF component (negative B_Y in the KSM frame and positive B_T in RTN) may restrict corotational motion of a newly opened field line in the northern dayside ionosphere [*Bunce et al*., 2005] as suggested by the annotation in Figure 6a. This is supported by the steady polarity of the IMF model estimates (positive B_T), the in situ Cassini IMF measurement on day 160 (negative B_Y), and the IMF polarity retained in the magnetosheath field measured by Cassini in the days leading up to the magnetopause crossing (negative B_Y). It is feasible that a significant transverse component of the IMF "held back" the auroral signature against corotation, resulting in the fixed local time position observed.

In addition to poleward motion, the UV intensity (up to 49 kR) and longevity ($>$2 h) of the spot signature are particularly notable. It is clear from Figures 4c and 4d that the spot was more intense in the early stages of its lifetime, before dimming, as it moved poleward over several hours. Note also the reduction in both size and UV power emission of the signature detailed in Table 1. We suggest that this is consistent with the convection of recently opened flux over the polar cap following reconnection at low latitude (as illustrated in Figure 6a), the reduction in emission power being proportional to the gradual depletion of any source particle population trapped on the convecting field line. Without particle measurements from Cassini this remains an interpretation, but we may now compare our observation with the expected emission power of an auroral cusp signature driven by low-latitude reconnection.

The model of *Bunce et al*. [2005] simulates the IMF control of Saturn's polar cusp aurora. Using typical electron population sources in the outer magnetosphere, plasma mantle, and lobe magnetosheath regions, *Knight* [1973] theory is used to derive the field-aligned voltages required to drive UV auroral emission through pulsed dayside reconnection at low- and high-latitude mapping positions, for varying IMF B_Y polarity. Table 2 compares the emission intensity and power of the spot observed here with *Bunce et al*. [2005] model estimates for "slow flow" solar wind conditions (applicable to periods of rarefaction and pertinent here). For simplicity, we quote only the upper model estimates of mean ($<I>$) and maximum (I_{MAX}) emission intensities, independent of the IMF B_Y orientation or source population provided by the *Bunce et al*. [2005] model, together with ranges of total emitted UV power for the low-latitude and high-latitude cases. Also listed in Table 2 are modeled and observed (values in brackets) parameters of polar cusp emissions at Saturn reported by *Gérard et al*. [2005], a study that adapted the *Bunce et al*. [2005] model to match observations made by HST. *Gérard et al*. [2005] found that significant increases of reconnection voltage and ionospheric flow speeds were required to bring the *Bunce et al*. [2005] estimates of UV intensity and power close to those observed by HST, suggesting that the lobe reconnection process may be more efficient at Saturn than predicted by the model. The lobe reconnection potential used in the *Bunce et al*. [2005] model was assumed to be half of that for low-latitude reconnection, based on the terrestrial study of *Milan et al*. [2004]. We attempt no such tailored comparison with the model here, noting only that the reconnection voltage of 200 kV proposed by *Gérard et al*. [2005] is more typically associated with compression-related levels on the dayside [*Jackman et al*., 2004], but here we have several indicators that the magnetosphere was not compressed (see section 4.1).

In Table 2 we provide the total UV power per nominal emission area of 10^{12} m^2, thereby accounting for the different areas of the cusp signature reported by the *Bunce et al*. [2005] and *Gérard et al*. [2005] studies. The spot area quoted in Table 3 for this study (1.6×10^{12} m^2) was calculated using the LT and latitude extents at 1843 UT in Table 2 and an approximation of 1000 km subtended per degree in the image. The total emitted power per area of the day 165 spot ranged between 0.46 and 1.96 GW/10^{12} m^2. Considering the low-latitude reconnection values (high-latitude reconnection is discussed in section 4.3), this is closer in magnitude to the adapted model estimate of *Gérard et al*. [2005], at 0.22–1.27 GW/10^{12} m^2, than the equivalent *Bunce et al*. [2005] estimate of 0.03–0.52 GW/10^{12} m^2 (particularly the upper end of the ranges). We note that the *Gérard et al*. [2005] study calculated emission power using the STIS UV bandwidth of 115–170 nm, i.e., not extrapolated over the unabsorbed wavelength range of H_2 emissions as per the *Gustin et al*. [2012] method used in this study. We therefore expect the *Gérard et al*. [2005] power values to be lower relative to those of this study by a factor of ~2 (factor for converting observed count rate to total unabsorbed H_2, divided by image exposure time). Taking this into account, the *Gérard et al*. [2005] observed value of 0.42 GW/10^{12} m^2 becomes a comparable 0.84 GW/10^{12} m^2. The maximum emitted power of the spot reported here was 1.96 GW/10^{12} m^2, confirming that it appears to have been more powerful per unit area than the *Bunce et al*. [2005] model predictions and previous cusp emissions observed with HST but comparable with the adapted low-latitude model case by *Gérard et al*. [2005] (up to 2.54 GW/10^{12} m^2). The comparisons in Table 2 are not direct, and the *Bunce et al*. [2005] model appears to underestimate the efficiency of dayside reconnection in producing auroral emissions as suggested by *Gérard et al*. [2005]; we include Table 2 as a summary review of similar case studies.

4.3. High-Latitude Dayside Reconnection

The auroral spot was located at high latitudes toward the end of the HST image sequence, with a poleward extent of only 4° colatitude (see Table 1). We consider here whether reconnection between the solar wind and planetary lobe flux could have driven the isolated spot emission. At Saturn this is more likely when upstream IMF is orientated southward, and the antiparallel reconnection site shifts away from low latitudes where the planetary field is also southward. Draped solar wind flux then reconnects with open lobe flux and is recirculated—initially equatorward—around the flanks in the direction of magnetosheath flow. Because no new open flux is produced, the overall OCB position remains unchanged; this process has been referred to as "lobe stirring" [e.g., *Reiff*, 1982; *Crooker*, 1992; *Bunce et al*., 2005]. We cannot say if this process was occurring in the southern hemisphere, although dual-hemispheric lobe reconnection is unlikely at Saturn due to the requirement for simultaneous and conjugate reconnection in each hemisphere [*Cowley et al*., 2008]. If this were the case, we would expect the aurora to appear initially just poleward of the OCB, before relaxing equatorward as the OCB reconfigures when open flux is closed. Terrestrial studies suggest that the lobe region is more susceptible to reconnection with draped IMF in the summer hemisphere, with a dependence on the IMF B_Y component [e.g., *Crooker and Rich*, 1993; *Lockwood and Moen*, 1999; *Fear et al*., 2015]; here we observed Saturn's northern hemisphere in spring, with a planetary axial tilt of ~22°.

How do we resolve the clear poleward motion of the spot if it was driven by lobe reconnection? Following single lobe reconnection, magnetic tension force is expected to initially contract the newly reconfigured open field line in a sunward direction, as it now threads the dayside magnetopause (e.g., see the terrestrial descriptions of *Reiff* [1982] or *Lockwood and Moen* [1999]). The particles undergoing auroral acceleration along this field line would therefore map as a signature with equatorward motion within the dayside cusp region of the ionosphere [e.g., *Milan et al*., 2000b], although any equatorward motion may be limited by the OCB position remaining effectively unchanged. Over a longer time scale, however, prolonged dayside lobe reconnection could successively reorder more poleward open lobe flux [e.g., *Doss et al*., 2015], resulting in an auroral signature that moves poleward from the OCB as observed here. Figure 6b provides a hypothetical sketch of this process, with red dots illustrating the multiple reconnection sites. We note, however, that the total emitted power of the spot reduced by a factor of 3–4 throughout its >2 h lifetime (attributed to both a decrease in the size of the spot and its brightness; see Table 1), whereas in the case of ongoing reconnection with magnetosheath field lines, we may expect the auroral spot to maintain a more stable brightness level if the source magnetosheath particle population was providing a relatively unchanged energy flux over 2 h.

It is possible for a strong IMF B_Y component to prevent the expected equatorward and duskward motion of the cusp spot resulting from a pulse of lobe reconnection, while precipitation of the accelerated plasma continues for several hours [*Bunce et al*., 2005; *Cowley et al*., 2005; *Meredith et al*., 2013]. We have already proposed that incidence of negative IMF B_Y fixed the spot emission in local time within the low-latitude reconnection scenario of section 4.2, but such IMF orientation would equally affect the motion of open flux at high latitude (see the terrestrial case of *Milan et al*. [2000b]), potentially more so since the plasma rotation effects evident in open flux production at the equator (e.g., subcorotation of auroral bifurcations [*Radioti et al*., 2011; *Badman et al*., 2013]) are not expected to be as dominant toward high latitudes [*Cowley and Bunce*, 2003; *Stallard et al*., 2004]. *Meredith et al*. [2014] attributed a high-latitude FUV emission in Saturn's northern aurora as a lobe signature (reaching up to the pole itself), supported by measurement of the incident southward IMF upstream by Cassini and a magnetic field model mapping the emission to open field lines [*Belenkaya et al*., 2014]. *Meredith et al*. [2014] also cited lack of corotation of the high-latitude spot being consistent with lobe reconnection.

We can again compare to the results of *Bunce et al*. [2005] and *Gérard et al*. [2005] shown in Table 2. The closest UV emission power compared to the spot observed here (0.46–1.96 GW/10^{12} m^2) is that of the high-latitude cusp emission observed by *Gérard et al*. [2005], which emitted 1.26 GW/10^{12} m^2, noting the factor ~2 adjustment for UV filter bandwidth discussed in section 4.1. Note that the emission area quoted from the *Gérard et al*. [2005] study (8.0×10^{12} m^2 for the high-latitude case) combines the *Bunce et al*. [2005] model region equatorward and poleward of the OCB and therefore the plasma mantle and magnetosheath source populations. The high reconnection voltages required to produce the *Gérard et al*. [2005] model estimates may also be excessive during periods of rarefaction as discussed previously.

4.4. Effect of Planetary Period Rotating Current Systems

Some element of the auroral spot's poleward motion could be attributed to ~ ±1° planetary period oscillation (PPO) of the entire northern oval position. This oval oscillation has been seen repeatedly in HST imagery from both hemispheres [*Nichols et al*., 2008, 2010, 2016]. The auroral oval is expected to be displaced equatorward in the direction of a region of rotating maximum upward PPO current [*Hunt et al*., 2015; *Badman et al*., 2016]. Indeed, modulation of the position of the southern cusp, associated with the PPO, has recently been observed in situ with Cassini [*Arridge et al*., 2016].

The spot intensity on day 165 appeared to increase (by at least a factor of 2) as the expected maximum northern PPO upward current rotated through the region, evident from the white crosses in Figures 4b and 4c (see the caption of Figure 4 for a description of PPO current annotation). If the upward rotating current sector were modulating the spot intensity, we expect an increase in emission intensity, at least toward the main emission latitudes where the PPO currents map. In terms of position, however, the expected oval oscillation would have shifted the upward FAC region equatorward and not poleward at this time. We note that the oval 1–2° oscillation magnitude occurs over a planetary period of ~10–11 h; here we observe a median poleward motion of ~4° in just 2 h. The possible modulation of the spot intensity by the northern PPO current system is notable, but oscillation of the oval associated with the PPOs does not appear to account for its movement toward the pole. It is also possible that the PPO systems could modulate magnetopause processes [e.g., *Clarke et al*., 2006]; however, the PPO currents discussed here flow at the main emission latitudes [e.g., *Hunt et al*., 2015], and the emission spot observed reaches notably higher latitudes, i.e., likely on open field lines.

5. Summary

We have examined a case of unusual UV auroral morphology in Saturn's northern hemisphere, observed by the HST STIS instrument on 14 June 2014 (day 165). The fading and eventual disappearance of the dawn arc was followed by the formation of an isolated and persistent high-latitude spot emission at postnoon local time. Present for at least 2 h, the spot moved poleward by a median ~4° latitude to a minimum colatitude of ~4°, remaining fixed in local time and displaying intensities of up to 49 kR. We systematically tracked the dawn arc and spot areas using image smoothing and intensity threshold contouring of unprojected images, allowing an estimate of emitted power to be made using the method of *Gustin et al*. [2012]. The maximum total emitted power of the isolated spot was 3.13 GW (corresponding to an area of ~1.6×10^{12} m^2),

which is significant considering the total auroral morphology emitted between 2.4 and 5.1 GW prior to the disappearance of the dawn arc.

Complete absence of the dawn arc is rarely observed at Saturn [e.g., *Gérard et al*., 2006]. Cassini crossed the magnetopause a few days prior to the observation window at an approximate subsolar standoff distance of between 24 and 27 R_S, indicating an expanded magnetosphere. A period of prolonged solar wind rarefaction was also indicated by in situ Cassini measurements and model projections from 1 AU. It is likely that the combination of an expanded magnetosphere and quiet solar wind led to the "switching off" of Saturn's dawn arc, through suppression of the rotational flow shear in the outer magnetosphere, in the absence of significant nightside reconnection- or plasma injection-driven sunward flows along the dawn flank. We note that this is different from the behavior of Jupiter's main auroral oval, which is driven by corotation enforcement currents in the middle magnetosphere [*Cowley and Bunce*, 2001], and is present under all solar wind conditions [*Clarke et al*., 2009; *Nichols et al*., 2009].

In this context we considered the potential reconnection scenarios that may have driven the isolated spot emission. The high latitude of the spot is consistent with either lobe or low-latitude reconnection, whereas its poleward motion is more easily explained by the relaxation of newly opened flux away from the OCB following low-latitude reconnection. The persistence of the spot for at least 2 h may put a useful lower time constraint on this convection process at Saturn. Given the particularly high latitude of the emission, we also considered the case for successive lobe reconnection at the far lobe driving the poleward motion, but the availability of a particle population source on older, open flux required to drive such a persistent emission is questionable. Comparison with previous modeled and observed polar cusp emissions from two studies, *Bunce et al*. [2005] and *Gérard et al*. [2005], confirmed that the observed spot was indeed a bright cusp emission signature, and perhaps closer to expectations for low-latitude reconnection driving rather than lobe reconnection, but the distinction is not clear.

The spot's fixed LT position may be attributed to negative IMF B_Y conditions incident at the time, combined with increased subcorotation of open flux toward higher latitudes. The emission intensity was also possibly enhanced by a sector of upward PPO current rotating through the region. These observations show conclusively that the mechanisms producing noon auroral spots and the "main oval" auroras (i.e., the dawn arc) are distinct, since in this case the cusp spot occurred without the arc. This finding thus supports in an independent way the previous inferences of *Radioti et al*. [2011], *Badman et al*. [2013], and *Meredith et al*. [2014]. These observations also suggest that reconnection can occur at an expanded magnetosphere, in agreement with the cusp observations of *Arridge et al*. [2016], who found evidence of reconnection under a range of upstream solar wind conditions.

Prolonged periods of rarefaction are expected during the declining phase of the current solar cycle. The unusual auroral morphology presented here, captured during what was likely a particularly quiet period of rarefaction, may be relevant in comparisons with any quieter auroral images obtained during the upcoming Cassini Grande Finale mission and its inclined orbits over Saturn's polar regions.

Acknowledgments

This work is based on observations made with the NASA/ESA Hubble Space Telescope (observation ID: GO13396), obtained at the Space Telescope Science Institute (STScI), which is operated by AURA, Inc., for NASA. The Hubble observations are available from the STScI website. J.K., S.V.B., and A.G. were supported by STFC grant ST/M001059/1. S.V.B. was also supported by an STFC Ernest Rutherford Fellowship ST/M005534/1. R.L.G. was supported by an STFC studentship. E.J. B., G.P., H.M., and S.W.H.C. were supported by STFC Consolidated grant ST/N000749/1. J.D.N. was supported by STFC Advanced Fellowship ST/1004084/1. We thank the Cassini MAG team at Imperial College London for access to processed magnetometer data, which are available online from the NASA PDS PPI node, and Bill Kurth (University of Iowa) for providing a description of the RPWS observations. The OMNI data were obtained from the GSFC/SPDF OMNIWeb interface at http://omniweb.gsfc.nasa.gov, and we thank K.C. Hansen and B. Zieger for providing solar wind propagations from their Michigan Solar Wind Model (http://mswim.engin.umich.edu/). Solar wind model projections from the *Tao et al.* [2005] model are available on request from C. Tao.

References

Achilleos, N., C. S. Arridge, C. Bertucci, C. M. Jackman, M. K. Dougherty, K. K. Khurana, and C. T. Russell (2008), Large-scale dynamics of Saturn's magnetopause: Observations by Cassini, *J. Geophys. Res.*, *113*, A11209, doi:10.1029/2008JA013265.

Andrews, D. J., A. J. Coates, S. W. H. Cowley, M. K. Dougherty, L. Lamy, G. Provan, and P. Zarka (2010), Magnetospheric period oscillations at Saturn: Comparison of equatorial and high-latitude magnetic field periods with north and south Saturn kilometric radiation periods, *J. Geophys. Res.*, *115*, A12252, doi:10.1029/2010JA015666.

Arridge, C. S., et al. (2016), Cassini observations of Saturn's southern polar cusp, *J. Geophys. Res. Space Physics*, *121*, 3006–3030, doi:10.1002/2015JA021957.

Badman, S. V., S. W. H. Cowley, L. Lamy, B. Cecconi, and P. Zarka (2008), Relationship between solar wind corotating interaction regions and the phasing and intensity of Saturn kilometric radiation bursts, *Ann. Geophys.*, *26*, 3641–3651, doi:10.5194/angeo-26-3641-2008.

Badman, S. V., et al. (2012), Rotational modulation and local time dependence of Saturn's infrared H_3^+ auroral intensity, *J. Geophys. Res.*, *117*, A09228, doi:10.1029/2012JA017990.

Badman, S. V., A. Masters, H. Hasegawa, M. Fujimoto, A. Radioti, D. Grodent, N. Sergis, M. K. Dougherty, and A. J. Coates (2013), Bursty magnetic reconnection at Saturn's magnetopause, *Geophys. Res. Lett.*, *40*, 1027–1031, doi:10.1002/grl.50199.

Badman, S. V., et al. (2016), Saturn's auroral morphology and field-aligned currents during a solar wind compression, *Icarus*, *263*, 83–93, doi:10.1016/j.icarus.2014.11.014.

Belenkaya, E. S., S. W. H. Cowley, C. J. Meredith, J. D. Nichols, V. V. Kalegaev, I. I. Alexeev, O. G. Barinov, W. O. Barinova, and M. S. Blokhina (2014), Magnetospheric magnetic field modelling for the 2011 and 2012 HST Saturn aurora campaigns—Implications for auroral source regions, *Ann. Geophys.*, *6*, 689–704, doi:10.5194/angeo-32-689-2014.

Bunce, E. J., S. W. H. Cowley, and S. E. Milan (2005), Interplanetary magnetic field control of Saturn's polar cusp aurora, *Ann. Geophys.*, *23*, 1405–1431, doi:10.5194/angeo-23-1405-2005.

Bunce, E. J., C. S. Arridge, S. W. H. Cowley, and M. K. Dougherty (2008), Magnetic field structure of Saturn's dayside magnetosphere and its mapping to the ionosphere: Results from ring current modeling, *J. Geophys. Res.*, *113*, A02207, doi:10.1029/2007JA012538.

Burton, M. E., M. K. Dougherty, and C. T. Russell (2010), Saturn's internal planetary magnetic field, *Geophys. Res. Lett.*, *37*, L24105, doi:10.1029/2010GL045148.

Cattaneo, M. B. B., C. Basile, G. Moreno, and J. D. Richardson (1998), Evolution of mirror structures in the magnetosheath of Saturn from the bow shock to the magnetopause, *J. Geophys. Res.*, *103*(A6), 11,961–11,972, doi:10.1029/97JA03683.

Clarke, J. T., et al. (2005), Morphological differences between Saturn's ultraviolet aurorae and those of Earth and Jupiter, *Nature*, *433*, 717–719, doi:10.1038/nature03331.

Clarke, J. T., et al. (2009), Response of Jupiter's and Saturn's auroral activity to the solar wind, *J. Geophys. Res.*, *114*, A05210, doi:10.1029/2008JA013694.

Clarke, K. E., et al. (2006), Cassini observations of planetary-period oscillations of Saturn's magnetopause, *Geophys. Res. Lett.*, *33*, L23104, doi:10.1029/2006GL027821.

Cowley, S. W. H., and E. J. Bunce (2001), Origin of the main auroral oval in Jupiter's coupled magnetosphere-ionosphere system, *Planet. Space Sci.*, *49*(10–11), 1067–1088, doi:10.1016/S0032-0633(00)00167-7.

Cowley, S. W. H., and E. J. Bunce (2003), Corotation-driven magnetosphere-ionosphere coupling currents in Saturn's magnetosphere and their relation to the auroras, *Ann. Geophys.*, *21*, 1691–1707, doi:10.5194/angeo-21-1691-2003.

Cowley, S. W. H., E. J. Bunce, and R. Prangé (2004), Saturn's polar ionospheric flows and their relation to the main auroral oval, *Ann. Geophys.*, *22*, 1379–1394, doi:10.5194/angeo-22-1379-2004.

Cowley, S. W. H., S. V. Badman, E. J. Bunce, J. T. Clarke, J.-C. Gérard, D. Grodent, C. M. Jackman, S. E. Milan, and T. K. Yeoman (2005), Reconnection in a rotation-dominated magnetosphere and its relation to Saturn's auroral dynamics, *J. Geophys. Res.*, *110*, A02201, doi:10.1029/2004JA010796.

Cowley, S. W. H., S. V. Badman, S. M. Imber, and S. E. Milan (2008), Comment on "Jupiter: A fundamentally different magnetospheric interaction with the solar wind" by D. J. McComas and F. Bagenal, *Geophys. Res. Lett.*, *35*, L10101, doi:10.1029/2007GL032645.

Crary, F. J., et al. (2005), Solar wind dynamic pressure and electric field as the main factors controlling Saturn's aurorae, *Nature*, *433*, 720–722, doi:10.1038/nature03333.

Crooker, N. U. (1992), Reverse convection, *J. Geophys. Res.*, *97*(A12), 19,363–19,372, doi:10.1029/92JA01532.

Crooker, N. U., and F. J. Rich (1993), Lobe cell convection as a summer phenomenon, *J. Geophys. Res.*, *98*(A8), 13,403–13,407, doi:10.1029/93JA01037.

Desroche, M., F. Bagenal, P. A. Delamere, and N. Erkaev (2013), Conditions at the magnetopause of Saturn and implications for the solar wind interaction, *J. Geophys. Res. Space Physics*, *118*, 3087–3095, doi:10.1002/jgra.50294.

Doss, C. E., C. M. Komar, P. A. Cassak, F. D. Wilder, S. Eriksson, and J. F. Drake (2015), Asymmetric magnetic reconnection with a flow shear and applications to the magnetopause, *J. Geophys. Res. Space Physics*, *120*, 7748–7763, doi:10.1002/2015JA021489.

Dougherty, M. K., et al. (2004), The Cassini magnetic field investigation, *Space Sci. Rev.*, *114*, 331–383, doi:10.1007/s11214-004-1432-2.

Dougherty, M. K., et al. (2005), Cassini magnetometer observations during Saturn orbit insertion, *Science*, *307*(5713), 1266–1270, doi:10.1126/science.1106098.

Dungey, J. W. (1961), Interplanetary magnetic field and the auroral zones, *Phys. Rev. Lett.*, *6*(2), 47–48, doi:10.1103/PhysRevLett.6.47.

Fear, R. C., S. E. Milan, J. A. Carter, and R. Maggiolo (2015), The interaction between transpolar arcs and cusp spots, *Geophys. Res. Lett.*, *42*, 9685–9693, doi:10.1002/2015GL066194.

Frey, H. U., S. B. Meade, T. J. Immel, S. A. Fuselier, E. S. Claflin, J.-C. Gérard, and B. Hubert (2002), Proton aurora in the cusp, *J. Geophys. Res.*, *107*(A7), 1091, doi:10.1029/2001JA900161.

Fuselier, S. A., H. U. Frey, K. J. Trattner, S. B. Mende, and J. L. Burch (2002), Cusp aurora dependence on interplanetary magnetic field B_Z, *J. Geophys. Res.*, *107*(A7), 111, doi:10.1029/2001JA900165.

Gérard, J.-C., E. J. Bunce, D. Grodent, S. W. H. Cowley, J. T. Clarke, and S. V. Badman (2005), Signature of Saturn's auroral cusp: Simultaneous Hubble Space Telescope FUV observations and upstream solar wind monitoring, *J. Geophys. Res.*, *110*, A11201, doi:10.1029/2005JA011094.

Gérard, J.-C., et al. (2006), Saturn's auroral morphology and activity during quiet magnetospheric conditions, *J. Geophys. Res.*, *111*, A12210, doi:10.1029/2006JA011965.

Gérard, J.-C., B. Bonfond, J. Gustin, D. Grodent, J. T. Clarke, D. Bisikalo, and V. Shematovich (2009), Altitude of Saturn's aurora and its implications for the characteristic energy of precipitated electrons, *Geophys. Res. Lett.*, *36*, L02202, doi:10.1029/2008GL036554.

Grodent, D., J. T. Clarke, J. Kim, J. H. Waite Jr., and S. W. H. Cowley (2003), Jupiter's main auroral oval observed with HST-STIS, *J. Geophys. Res.*, *108*(A11), 1389, doi:10.1029/2003JA009921.

Grodent, D., J.-C. Gérard, S. W. H. Cowley, E. J. Bunce, and J. T. Clarke (2005), Variable morphology of Saturn's southern ultraviolet aurora, *J. Geophys. Res.*, *110*, A07215, doi:10.1029/2004JA010983.

Gustin, J., B. Bonfond, D. Grodent, and J.-C. Gérard (2012), Conversion from HST ACS and STIS auroral counts into brightness, precipitated power, and radiated power for H_2 giant planets, *J. Geophys. Res.*, *117*, A07316, doi:10.1029/2012JA017607.

Jackman, C. M., N. Achilleos, E. J. Bunce, S. W. H. Cowley, M. K. Dougherty, G. H. Jones, S. E. Milan, and E. J. Smith (2004), Interplanetary magnetic field at ~9 AU during the declining phase of the solar cycle and its implications for Saturn's magnetospheric dynamics, *J. Geophys. Res.*, *109*, A11203, doi:10.1029/2004JA010614.

Hunt, G. J., S. W. H. Cowley, G. Provan, E. J. Bunce, I. I. Alexeev, E. S. Belenkaya, V. V. Kalegaev, M. K. Dougherty, and A. J. Coates (2014), Field-aligned currents in Saturn's southern nightside magnetosphere: Subcorotation and planetary period oscillation components, *J. Geophys. Res. Space Physics*, *119*, 9847–9899, doi:10.1002/2014JA020506.

Hunt, G. J., S. W. H. Cowley, G. Provan, E. J. Bunce, I. I. Alexeev, E. S. Belenkaya, V. V. Kalegaev, M. K. Dougherty, and A. J. Coates (2015), Field-aligned currents in Saturn's northern nightside magnetosphere: Evidence for interhemispheric current flow associated with planetary period oscillations, *J. Geophys. Res. Space Physics*, *120*, 7552–7584, doi:10.1002/2015JA021454.

Jasinski, J. M., et al. (2014), Cusp observation at Saturn's high-latitude magnetosphere by the Cassini spacecraft, *Geophys. Res. Lett.*, *41*, 1382–1388, doi:10.1002/2014GL059319.

Jasinski, J. M., J. A. Slavin, C. S. Arridge, G. Poh, X. Jia, N. Sergis, A. J. Coates, G. H. Jones, and J. H. Waite Jr. (2016), Flux transfer event observation at Saturn's dayside magnetopause by the Cassini spacecraft, *Geophys. Res. Lett.*, *43*, 6713–6723, doi:10.1002/2016GL069260.

Jinks, S. L., et al. (2014), Cassini multi-instrument assessment of Saturn's polar cap boundary, *J. Geophys. Res. Space Physics*, *119*, 8161–8177, doi:10.1002/2014JA020367.

Joy, S. P., M. G. Kivelson, R. J. Walker, K. K. Khurana, C. T. Russell, and W. R. Paterson (2006), Mirror mode structures in the Jovian magnetosheath, *J. Geophys. Res.*, *111*, A12212, doi:10.1029/2006JA011985.

Kanani, S. J., et al. (2010), A new form of Saturn's magnetopause using a dynamic pressure balance model, based on in situ, multi-instrument Cassini measurements, *J. Geophys. Res.*, *115*, A06207, doi:10.1029/2009JA014262.

Knight, S. (1973), Parallel electric fields, *Planet. Space Sci.*, *21*, 741–751.

Lamy, L., R. Prangé, W. Pryor, J. Gustin, S. V. Badman, H. Melin, T. Stallard, D. G. Mitchell, and P. C. Brandt (2013), Multispectral simultaneous diagnosis of Saturn's aurorae throughout a planetary rotation, *J. Geophys. Res. Space Physics*, *118*, 4817–4843, doi:10.1002/jgra.50404.

Lockwood, M., and J. Moen (1999), Reconfiguration and closure of lobe flux by reconnection during northward IMF: Possible evidence for signatures in cusp/cleft auroral emissions, *Ann. Geophys.*, *17*(8), 996–1011, doi:10.1007/s005850050827.

Masters, A., J. P. Eastwood, M. Swisdak, M. F. Thomsen, C. T. Russell, N. Sergis, F. J. Crary, M. K. Dougherty, A. J. Coates, and S. M. Krimigis (2012), The importance of plasma β conditions for magnetic reconnection at Saturn's magnetopause, *Geophys. Res. Lett.*, *39*, L08103, doi:10.1029/2012GL051372.

McAndrews, H. J., C. J. Owen, M. Thomsen, B. Lavraud, A. Coates, M. Dougherty, and D. T. Young (2008), Evidence for reconnection at Saturn's magnetopause, *J. Geophys. Res.*, *113*, A04210, doi:10.1029/2007JA012581.

Meredith, C. J., S. W. H. Cowley, K. C. Hansen, J. D. Nichols, and T. K. Yeoman (2013), Simultaneous conjugate observations of small-scale structures in Saturn's dayside ultraviolet auroras: Implications for physical origins, *J. Geophys. Res. Space Physics*, *118*, 2244–2266, doi:10.1002/jgra.50270.

Meredith, C. J., I. I. Alexeev, S. V. Badman, E. S. Belenkaya, S. W. H. Cowley, M. K. Dougherty, V. V. Kalegaev, G. R. Lewis, and J. D. Nichols (2014), Saturn's dayside ultraviolet auroras: Evidence for morphological dependence on the direction of the upstream interplanetary magnetic field, *J. Geophys. Res. Space Physics*, *119*, 1994–2008, doi:10.1002/2013JA019598.

Meredith, C. J., C. J. Meredith, S. W. H. Cowley, and J. D. Nichols (2015), Survey of Saturn auroral storms observed by the Hubble Space Telescope: Implications for storm time scales, *J. Geophys. Res. Space Physics*, *119*, 9624–9642, doi:10.1002/2014JA020601.

Milan, S. E., M. Lester, S. W. H. Cowley, and M. Brittnacher (2000a), Convection and auroral response to a southward turning of the IMF: Polar UVI, CUTLASS, and IMAGE signatures of transient magnetic flux transfer at the magnetopause, *J. Geophys. Res.*, *105*(A7), 15,741–15,755, doi:10.1029/2000JA900022.

Milan, S. E., M. Lester, S. W. H. Cowley, and M. Brittnacher (2000b), Dayside convection and auroral morphology during an interval of northward interplanetary magnetic field, *Ann. Geophys.*, *18*, 436–444, doi:10.1007/s00585-000-0436-9.

Milan, S. E., S. W. H. Cowley, M. Lester, D. M. Wright, J. A. Slavin, M. Fillingim, C. W. Carlson, and H. J. Singer (2004), Response of the magnetotail to changes in the open flux content of the magnetosphere, *J. Geophys. Res.*, *109*, A04220, doi:10.1029/2003JA010350.

Milan, S. E., et al. (2010), Average auroral configuration parameterized by geomagnetic activity and solar wind conditions, *Ann. Geophys.*, *28*(4), 1003–1012, doi:10.5194/angeo-28-1003-2010.

Mitchell, D. G., et al. (2009), Recurrent energization of plasma in the midnight-to-dawn quadrant of Saturn's magnetosphere, and its relationship to auroral UV and radio emissions, *Planet. Space Sci.*, *57*(14–15), 1732–1742, doi:10.1016/j.pss.2009.04.002.

Mitchell, D. G., J. F. Carbary, E. J. Bunce, A. Radioti, S. V. Badman, W. R. Pryor, G. B. Hospodarsky, and W. S. Kurth (2016), Recurrent pulsations in Saturn's high latitude magnetosphere, *Icarus*, *263*, 94–100, doi:10.1016/j.icarus.2014.10.028.

Nichols, J. D., J. T. Clarke, S. W. H. Cowley, J. Duval, A. J. Farmer, J.-C. Gérard, D. Grodent, and S. Wannawichian (2008), Oscillation of Saturn's southern auroral oval, *J. Geophys. Res.*, *113*, A11205, doi:10.1029/2008JA013444.

Nichols, J. D., J. T. Clarke, J. C. Gérard, D. Grodent, and K. C. Hansen (2009), Variation of different components of Jupiter's auroral emission, *J. Geophys. Res.*, *114*, A06210, doi:10.1029/2009JA014051.

Nichols, J. D., S. W. H. Cowley, and L. Lamy (2010), Dawn-dusk oscillation of Saturn's conjugate auroral ovals, *Geophys. Res. Lett.*, *37*, L24102, doi:10.1029/2010GL045818.

Nichols, J. D., et al. (2014), Dynamic auroral storms on Saturn as observed by the Hubble Space Telescope, *Geophys. Res. Lett.*, *41*, 3323–3330, doi:10.1002/2014GL060186.

Nichols, J. D., S. V. Badman, E. J. Bunce, J. T. Clarke, S. W. H. Cowley, G. J. Hunt, and G. Provan (2016), Saturn's northern auroras as observed using the Hubble Space Telescope, *Icarus*, *263*, 17–31, doi:10.1016/j.icarus.2015.09.008.

Øieroset, M., P. E. Sandholt, W. F. Denig, and S. W. H. Cowley (1997), Northward interplanetary magnetic field cusp aurora and high-latitude magnetopause reconnection, *J. Geophys. Res.*, *102*(A6), 11,349–11,362, doi:10.1029/97JA00559.

Palmaerts, B., A. Radioti, E. Roussos, D. Grodent, J.-C. Gérard, N. Krupp, and D. G. Mitchell (2016), Pulsations of the polar cusp aurora at Saturn, *J. Geophys. Res. Space Physics*, *121*, 11,952–11,963, doi:10.1002/2016JA023497.

Pilkington, N. M., N. Achilleos, C. S. Arridge, P. Guio, A. Masters, L. C. Ray, N. Sergis, M. F. Thomsen, A. J. Coates, and M. K. Dougherty (2015), Internally driven large-scale changes in the size of Saturn's magnetosphere, *J. Geophys. Res. Space Physics*, *120*, 7289–7306, doi:10.1002/2015JA021290.

Provan, G., D. J. Andrews, C. S. Arridge, A. J. Coates, S. W. H. Cowley, S. E. Milan, M. K. Dougherty, and D. M. Wright (2009), Polarization and phase of planetary-period magnetic field oscillations on high-latitude field lines in Saturn's magnetosphere, *J. Geophys. Res.*, *114*, A02225, doi:10.1029/2008JA013782.

Provan, G., S. W. H. Cowley, L. Lamy, E. J. Bunce, G. J. Hunt, P. Zarka, and M. K. Dougherty (2016), Planetary period oscillations in Saturn's magnetosphere: Coalescence and reversal of northern and southern periods in late northern spring, *J. Geophys. Res. Space Physics*, *121*, 9829–9862, doi:10.1002/2016JA023056.

Radioti, A., D. Grodent, J.-C. Gérard, S. E. Milan, B. Bonfond, J. Gustin, and W. Pryor (2011), Bifurcations of the main auroral ring at Saturn: Ionospheric signatures of consecutive reconnection events at the magnetopause, *J. Geophys. Res.*, *116*, A11209, doi:10.1029/2011JA016661.

Radioti, A., D. Grodent, J.-C. Gérard, B. Bonfond, J. Gustin, W. Pryor, J. M. Jasinski, and C. S. Arridge (2013), Auroral signatures of multiple magnetopause reconnection at Saturn, *Geophys. Res. Lett.*, *40*, 4498–4502, doi:10.1002/grl.50889.

Radioti, A., D. Grodent, J.-C. Gérard, S. E. Milan, R. C. Fear, C. M. Jackman, B. Bonfond, and W. Pryor (2014), Saturn's elusive nightside polar arc, *Geophys. Res. Lett.*, *41*, 6321–6328, doi:10.1002/2014GL061081.

Radioti, A., D. Grodent, X. Jia, J.-C. Gérard, B. Bonfond, W. Pryor, J. Gustin, D. G. Mitchell, and C. M. Jackman (2016), A multi-scale magnetotail reconnection event at Saturn and associated flows: Cassini/UVIS observations, *Icarus*, *263*, 75–82, doi:10.1016/j.icarus.2014.12.016.

Reiff, P. H. (1982), Sunward convection in both polar caps, *J. Geophys. Res.*, *87*(A8), 5976–5980, doi:10.1029/JA087iA08p05976.

Sanchez-Diaz, E., A. P. Rouillard, B. Lavraud, K. Segura, C. Tao, R. Pinto, N. R. Jr Sheeley, and I. Plotnikov (2016), The very slow solar wind: Properties, origin and variability, *J. Geophys. Res. Space Physics*, *121*, 2830–2841, doi:10.1002/2016JA022433.

Stallard, T. S., S. Miller, L. M. Trafton, T. R. Geballe, and R. D. Joseph (2004), Ion winds in Saturn's southern auroral/polar region, *Icarus*, *167*(1), 204–211, doi:10.1016/j.icarus.2003.09.006.

Talboys, D. L., C. S. Arridge, E. J. Bunce, A. J. Coates, S. W. H. Cowley, and M. K. Dougherty (2009), Characterization of auroral current systems in Saturn's magnetosphere: High-latitude Cassini observations, *J. Geophys. Res.*, *114*, A06220, doi:10.1029/2008JA013846.

Tao, C., R. Kataoka, H. Fukunishi, Y. Takahashi, and T. Yokoyama (2005), Magnetic field variations in the Jovian magnetotail induced by solar wind dynamic pressure enhancements, *J. Geophys. Res.*, *110*, A11208, doi:10.1029/2004JA010959.

Zeiger, B., and K. C. Hansen (2008), Statistical validation of a solar wind propagation model from 1 to 10 AU, *J. Geophys. Res.*, *113*, A08107, doi:10.1029/2008JA013046.